



Research on thermal design and thermal optical performance of space telescope based on multidisciplinary integration

Zhipeng Yuan, Xu Meng, Chengliang Li, Mengmeng Xu & Liheng Chen

To cite this article: Zhipeng Yuan, Xu Meng, Chengliang Li, Mengmeng Xu & Liheng Chen (2022) Research on thermal design and thermal optical performance of space telescope based on multidisciplinary integration, Journal of Thermal Stresses, 45:5, 401-414, DOI: [10.1080/01495739.2022.2049023](https://doi.org/10.1080/01495739.2022.2049023)

To link to this article: <https://doi.org/10.1080/01495739.2022.2049023>



Published online: 30 Mar 2022.



Submit your article to this journal [↗](#)



Article views: 55





View related articles [↗](#)



View Crossmark data [↗](#)



Research on thermal design and thermal optical performance of space telescope based on multidisciplinary integration

Zhipeng Yuan^{a,b} , Xu Meng^{a,b}, Chengliang Li^a, Mengmeng Xu^a, and Liheng Chen^a 

^aChangchun Institute of Optics, Fine Mechanics and Physics, Chinese Academy of Sciences, Changchun, China; ^bUniversity of Chinese Academy of Sciences, Beijing, China

ABSTRACT

This paper first analyzes the external heat flow of a low-orbit space telescope in different flight attitudes, and determines the position of the heat dissipation surface and the thermal analysis cases. Then, the detailed thermal design of each component of the telescope is completed to reduce the influence of thermal deformation of optical elements and supporting structures caused by temperature changes on the imaging quality of telescope. Especially for the thermal control difficulties of CCD detectors such as large heat generation in a short time and one-dimensional movement in a narrow space, a segmented proprietary cold chain with flexible section is designed to transfer the heat to the radiant cold plate. Finally, the thermal/structure/optical integrated simulation analysis under extreme cases is carried out. It is concluded that the average modulation transfer function (MTF) of the optical system at the cutoff frequency satisfies the design requirement greater than 0.3. The analysis results show that the thermal control system designed in this paper can ensure the optical performance of the telescope, which has important reference significance for the thermal design of other space telescopes.

ARTICLE HISTORY

Received 18 October 2021
Accepted 20 November 2021

KEYWORDS

Space telescope; thermal control system; thermal design; thermal/structural/optical analysis

1. Introduction

With the continuous development of space-to-earth observation technology, low-earth orbit space telescopes have played an important role in many fields such as resource surveys, environmental monitoring, topographic mapping, atmospheric and ocean observation, and military reconnaissance [1].

However, space telescopes operating in low earth orbit will be alternately affected by solar radiation, earth infrared radiation, earth albedo, cold black space and internal heat source, resulting in uneven temperature of internal optical elements and support structures, which will cause thermal deformation of optical element surfaces and support structures and greatly reduce the imaging quality [2–4]. To ensure the good imaging quality of space telescope, researchers have conducted many studies on its thermal control system. Gao et al. [5] completed the thermal design and thermal analysis of the camera based on the thermal control indicators of the high-resolution MWIR/LWIR aerial camera to ensure that the aerial camera meets working requirements under complex external conditions. Li et al. [6] designed a high-precision and high-stability thermal control system for Chinese GF-4 remote sensing satellite, which achieved the high resolution and sensitivity required for scientific observation. M. Mueller et al. [7] discussed the MK-level precision thermal control design of the G-CLEF spectrometer and focal plane. Li [8–10] used MATLAB to calculate the complex external heat flow under

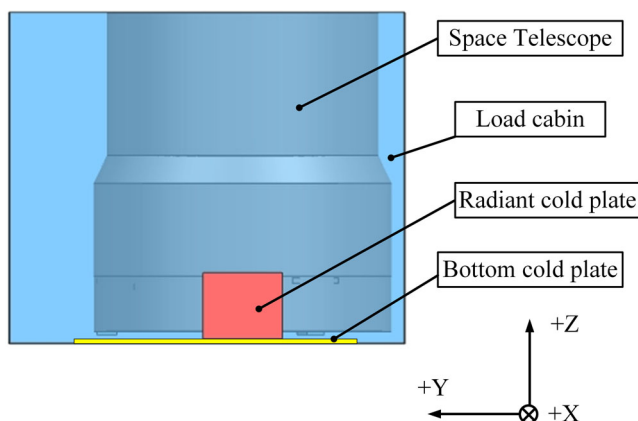


Figure 1. Overall structure of telescope.

the condition of constant attitude and two-dimensional variable attitude in an orbit cycle. According to the specific requirements of solar X-ray and extreme ultraviolet imager for the temperature of optical system, the thermal control scheme of CCD and imager was designed in detail, and its rationality was verified by thermal balance test.

The above studies have carried out the corresponding thermal design according to the thermal control requirements of space optical remote sensor and its components. However, these studies take the temperature of each component as the evaluation index, ignoring the change of the optical performance of the system under the action of the comprehensive temperature field. In this paper, the thermal control system of a low earth orbit space telescope is designed in detail according to its performance requirements and the thermal control difficulties of each component. Then, the thermal/structural/optical analysis under two extreme cases is carried out to explore the optical performance of the telescope system under the predicted temperature field [11, 12]. Finally, the rationality of the thermal control system is verified by the optical performance index.

2. Telescope overview

2.1. The structure of the telescope

The telescope is mounted on the bottom cold plate at the bottom of the load cabin through titanium alloy support. The overall structure of the telescope is shown in Figure 1. Except for the light entrance, the load cabin is covered by a shell.

It mainly includes optical elements such as primary mirror, secondary mirror, and three mirrors, and a supporting structure composed of a secondary mirror support, a rear frame and telescope supports, and electric boxes installed on the rear frame.

2.2. Performance indicators of the telescope

In order to ensure the good optical performance of the telescope, the average MTF of the telescope optical system at the cutoff frequency is required to be greater than 0.3. CCD and electronic components are precision components, the extreme temperature will affect their normal working performance. Therefore, the thermal control index of CCD and electric boxes is given: 0–30 °C for CCD detector and –10–40 °C for electric boxes.

Table 1. External heat flow analysis cases and analysis results.

Case name	Case definition		Orbital period average external heat flow (W/m ²)		
	Flight attitude (°)	β (°)	Light entrance	-X surface	-Y surface
1	Pitch angle 0, roll angle 0	+66	330.76	212.15	724.00
2	Pitch angle 0, roll angle 0	0	347.78	327.61	104.88
3	pitch angle 0, roll angle 0	-66	330.81	212.17	79.64
4	Pitch angle +10, roll angle 0	+66	330.88	215.86	657.90
5	Pitch angle +10, roll angle 0	0	358.20	276.96	104.89
6	Pitch angle +10, roll angle 0	-66	330.93	215.88	79.65
7	Pitch angle -10, roll angle 0	+66	330.60	172.65	657.89
8	Pitch angle -10, roll angle 0	0	359.14	291.39	104.87
9	Pitch angle -10, roll angle 0	-66	330.65	172.66	79.63
10	Roll angle +10, pitch angle 0	+66	254.04	169.26	560.03
11	Roll angle +10, pitch angle 0	0	335.58	313.59	155.76
12	Roll angle +10, pitch angle 0	-66	452.25	233.93	114.02
13	Roll angle -10, pitch angle 0	+66	452.26	233.95	903.01
14	Roll angle -10, pitch angle 0	0	335.65	313.64	92.31
15	Roll angle -10, pitch angle 0	-66	254.15	174.32	49.51

3. The thermal environment of the telescope

3.1. Thermal environment analysis

The telescope works in a typical circular orbit in low earth orbit, and it will be alternately affected by external heat flows such as solar radiation, earth albedo, earth infrared radiation and cold black space. In addition, the boundary temperature is also an important external input condition of the telescope, including the load cabin temperature of -20 – 40 °C and the bottom cold plate temperature of 0 – 28 °C. Finally, the heat generated by the internal heat source is also one of the main factors affecting the operating temperature of the telescope. The power consumption of CCD is 3.5 W, and electric boxes are also the main heat source.

Assuming that the +X direction of the telescope points to the flight direction, the +Z direction points to the earth, and the +Y direction is determined according to the right-hand rule. In addition, when the telescope works in orbit, it will perform a small angle offset based on the above-mentioned flight attitude according to the observation needs, and the deflection angle does not exceed $\pm 10^\circ$. It is defined that the pitch angle is positive when the +Z axis rotates to the +X axis, and the roll angle is positive when the +Z axis rotates to the +Y axis.

3.2. External heat flow analysis

As the external input of the space telescope, the external heat flow not only affects the temperature level of its internal optical system and supporting structure, but an accurate and reliable external heat flow is also a prerequisite and guarantee for reasonable thermal design, thermal simulation and correct thermal test [13]. According to the orbital parameters of the telescope, it is calculated that within a year, the β angle changes periodically between $+66^\circ$ and -66° . The external heat flow analysis cases are defined according to the β angle and the flight attitude. The β angle is taken as $+66^\circ$, -66° and 0° , and the pitch angle and roll angle are taken as $+10^\circ$, 0° and -10° , respectively. A total of 15 external heat flow analysis cases are defined, and the minimum solar constant is 1322 W/m². As the telescope is installed inside the load, other instruments are installed in the +X and +Y directions, which is not conducive to the opening of the heat dissipation surface. Therefore, only the orbital periodic average external heat flux received by the -X surface, -Y surface and the light entrance (+Z surface) is analyzed. According to the defined external heat flow analysis cases, the thermal analysis software UG/NX Space System Thermal (hereinafter referred to as UG/NX SST) is used for thermal simulation analysis to obtain the

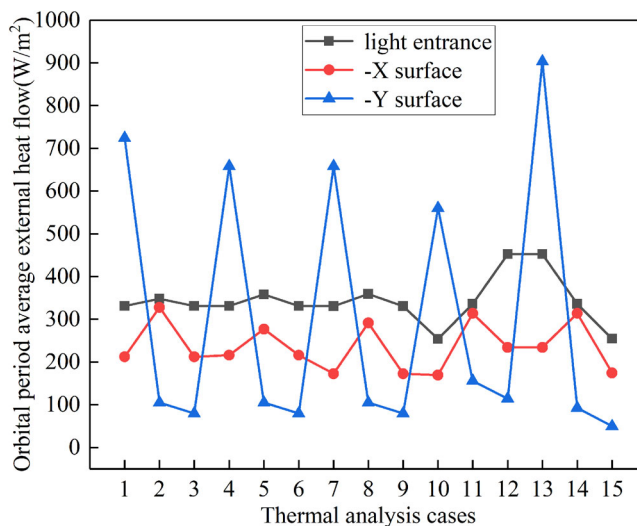


Figure 2. Orbital period average external heat flow under 15 cases.

average external heat flow value of the orbital period received by the light entrance, -X surface and -Y surface, as shown in Table 1. Figure 2 shows the corresponding graph.

It can be seen from Figure 2 that the average external heat flow received by the -Y surface of the telescope under different cases fluctuates greatly, and it receives more direct solar heat flow under extreme β angle conditions. The average external heat flow received by the -X surface under different cases is small and relatively stable, so it is more reasonable to choose the -X surface as the heat dissipation surface.

According to Table 1, it can be seen that the maximum and minimum average external heat flow received by the heat dissipation surface are case 2 and case 10, respectively. Therefore, the flight attitude and β angle of case 2 and case 10 are respectively defined as the flight attitude and β angle of thermal analysis hot case and cold case.

4. Design of thermal control system

The thermal control system of the space telescope is mainly used to maintain the working temperature of the optical system and mechanical structure to ensure that it has good optical performance in a complex thermal environment. The stable thermal design can maintain the performance of the optical system in a variety of extreme thermal environments through multi-layer insulation assembly (MLI), insulation pads, heat conducting cable, coating, and pasting heating sheets and temperature sensors.

4.1. Optical system

To reduce the influence of the load cabin on the optical system, 15-units MLI are covered on the outer surface of the lens barrel. Each unit is composed of a layer of double-sided aluminized polyester film reflective screen and a layer of polyester mesh. And heating sheets are pasted on the surface of the lens barrel to maintain the temperature level of the lens barrel.

The primary mirror is the most important optical element in the optical system, and its temperature change has a greater impact on the imaging quality of the system. Therefore, an aluminum alloy radiant heating plate is installed on the back of the primary mirror. The radiation

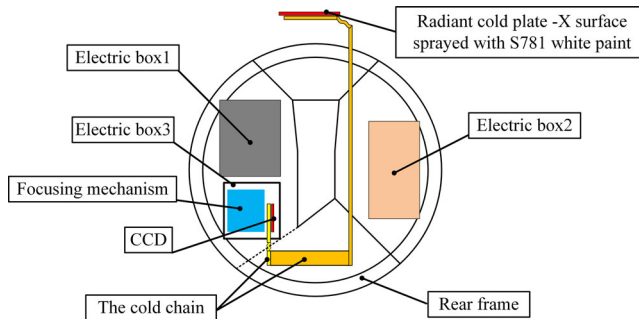


Figure 3. Schematic diagram of CCD thermal design.

heating plate is blackened and heating sheets are pasted on its back to maintain the working temperature of the primary mirror by enhancing radiation heat transfer.

To ensure the temperature of the secondary mirror, an aluminum alloy heating cover is set. The surface of the heating cover is blackened, and heating sheets are pasted on its surface to maintain the temperature level of the secondary mirror through radiation and heat conduction. The outer surface of the heating cover is covered with MLI, and the outermost layer is covered with anti-atomic oxygen cloth to reduce the influence of external heat flow and atomic oxygen. A heating sheet is pasted on the surface of the secondary mirror support and covered with MLI to ensure the temperature of the secondary mirror support. In addition, in order to eliminate the influence of stray light, polyimide black carburized film is used on the surface of MLI.

4.2. Rear frame

The temperature of the rear frame is maintained by radiation and heat transfer with the rear frame cover installed at the bottom. To enhance the radiation heat transfer, the surface of the rear frame structure and the surface of the rear frame cover are blackened. The outer surface of the rear frame cover is pasted with a heating sheet and covered with MLI and the surface film uses a low-emissivity aluminum-plated polyester film to reduce the radiation effect of the bottom cold plate and the load cabin.

4.3. CCD detector assembly

As a precision component that converts optical signals into electrical signals, CCD has higher requirements for operating temperature. However, the power consumption of the CCD is 3.5 W when it is working, and it generates a lot of heat in a short period of time. In addition, the internal space of the electric box3 is small and the external components such as the electric box1, the electric box2, and the rear frame affect the planning of the heat dissipation path. These factors have brought great challenges to thermal design. To ensure the working temperature of the CCD and the one-dimensional movement in a narrow space, a segmented proprietary cold chain with flexible sections is designed to guide the excess heat to the radiant cold plate, as shown in Figure 3.

The specific thermal design is as follows:

1. The first section of the cold chain is designed with a flexible section to ensure the one-dimensional movement of the CCD;
2. Each installation interface of the cold chain is filled with heat conducting silicone grease to reduce the thermal resistance on the heat dissipation path;

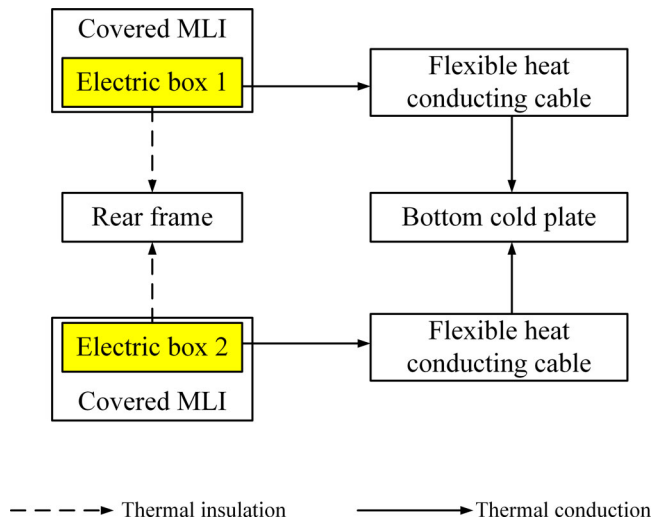


Figure 4. Schematic diagram of electric box thermal design.

3. The radiation cold plate is installed on the load frame with four 8 mm thick polyimide insulation pads;
4. S781 white paint is sprayed on the -X surface of the radiation cold plate to increase radiation heat dissipation. At the same time, the heating sheet is pasted on the +X side to ensure the temperature of the radiation cold plate when the CCD is not working;
5. The cold chain is installed on the rear frame through 4 titanium alloy supports. The outer surface of the cold chain is covered with MLI, and the outermost layer is aluminized polyester film to reduce the influence of surrounding components.

4.4. Electric box

Since the main heating element CCD in the electric box3 dissipates heat through a proprietary heat dissipation channel, the thermal design of the electric box includes the thermal design of electric box1 and electric box2. When electric box1 and electric box2 work, the heat of internal electronic components is guided to the shell of the electric box through the heat-conducting aluminum block, and then the heat is guided to the bottom cold plate by flexible heat-conducting cable to dissipate heat. The connection interface is filled with heat conducting silicone grease, as shown in Figure 4. To reduce the influence of the temperature of the electric box on the surrounding components, the electric box is installed on the rear frame through four 10 mm thick polyimide insulation pads. The outer surface of the electric box is covered with MLI, and the surface film is made of aluminized polyester film.

5. Integrated simulation analysis

In order to accurately understand the optical performance of the space telescope under a complex thermal environment, it is necessary to conduct thermal/structural/optical analysis. Figure 5 shows the flow of thermal/structural/optical integrated analysis of the space telescope. The thermal analysis module predicts the temperature field of the telescope in orbit, the structural analysis module predicts the deformation under the action of the above temperature field, and the optical analysis module predicts the optical performance of the deformed system.

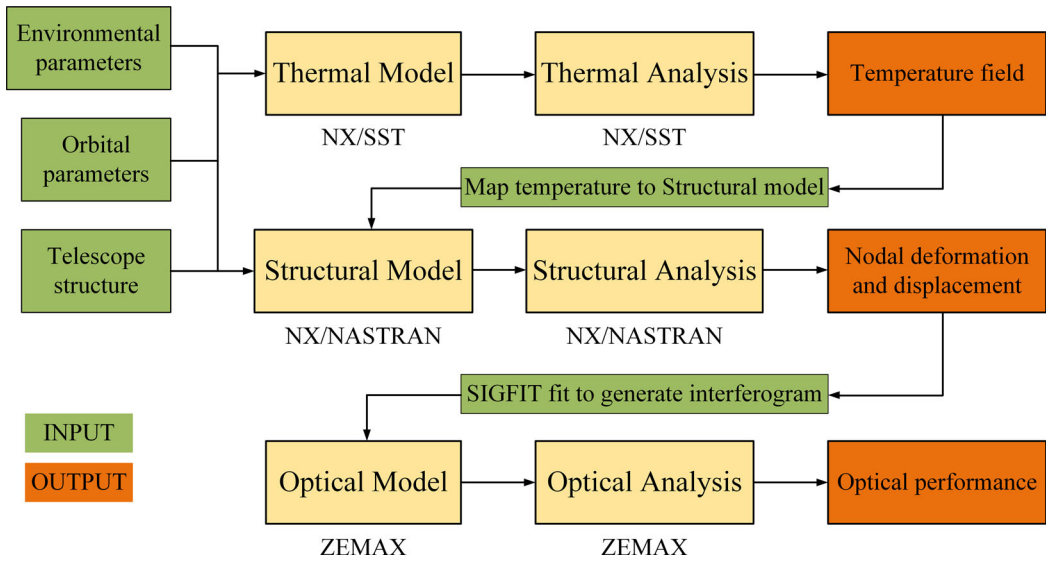


Figure 5. Thermal/structural/optical integrated analysis flow chart.

5.1. Thermal analysis

Thermal analysis is a key step to accurately predict the temperature distribution of the telescope in extreme environments. The results produced have a profound impact on the deformation and displacement of the telescope support structure and optical components, thereby affecting the optical performance of the system.

5.1.1. Establishment of thermal analysis model

The thermal model of the telescope is established using the UG/NX SST module, as shown in Figure 6. Figure 6(a) and 6(b) shows the telescope system and the internal optical components, respectively.

In order to save computing time and resources, the following simplifications are made:

1. All components of the telescope are meshed with two-dimensional shell elements, and the element thickness is calculated according to the volume equivalent thickness.
2. Heat conduction between components is simplified by thermal coupling.

According to the law of energy conservation, the sum of the heat flowing into node j and its own heating should be equal to the sum of the heat flowing out of node j and its internal energy increment. The heat balance equation of any node j of the telescope is established, as shown in formula (1).

$$Q_{sj} + Q_{pj} + Q_{rj} + Q_{dj} = Q_{cj} + Q_{fj} \quad (1)$$

where Q_{sj} is the heat flow outside the space absorbed by node j ; Q_{pj} is the heat generated by node j itself; Q_{rj} is the radiant heat of node i to node j ; Q_{dj} is the conduction heat between node j and node i ; Q_{cj} is the internal energy increment of node j and is a function of time; Q_{fj} is the heat radiated outward by node j . Node j conducts radiation heat exchange with the outside world through formulas (2), (3), and (4).

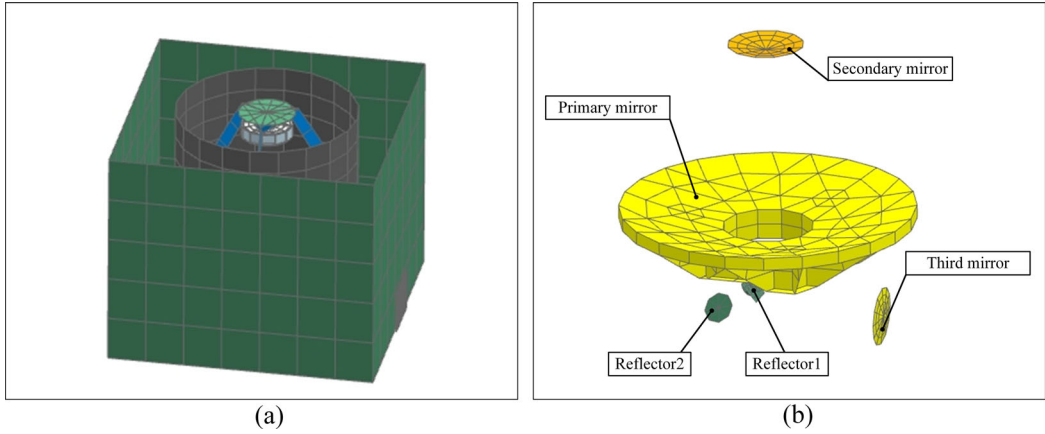


Figure 6. Thermal model of telescope: (a) telescope system, (b) optical components.

$$Q_{sj} = (\alpha_{sj}S\varphi_{1,j} + \alpha_{sj}E_a\varphi_{2,j} + \varepsilon_jE_e\varphi_{3,j})A_j \quad (2)$$

$$Q_{rj} = \sum_{i=1}^m B_{i,j}A_i\varepsilon_i\sigma T_i^4 \quad (3)$$

$$Q_{fj} = A_j\varepsilon_j\sigma T_j^4 \quad (4)$$

where α_{sj} is the solar absorptivity of node j ; S is the solar constant; E_a is the earth's average albedo intensity; E_e is the earth's average infrared radiation intensity; $\varphi_{1,j}$, $\varphi_{2,j}$ and $\varphi_{3,j}$ are the geometric angle coefficient of node j relative to the sun, the earth's albedo and the earth's infrared radiation, respectively; $B_{i,j}$ is the Gebhart coefficient; σ is the Stefan-Boltzmann constant; A_i , ε_i and T_i are the surface area, infrared emissivity and temperature of node i , respectively; A_j , ε_j , T_j are the surface area, infrared emissivity and temperature of node j , respectively. Node j conducts conduction heat exchange with other nodes through formula (5).

$$Q_{dj} = \sum_{i=1}^n D_{i,j}(T_j - T_i) \quad (5)$$

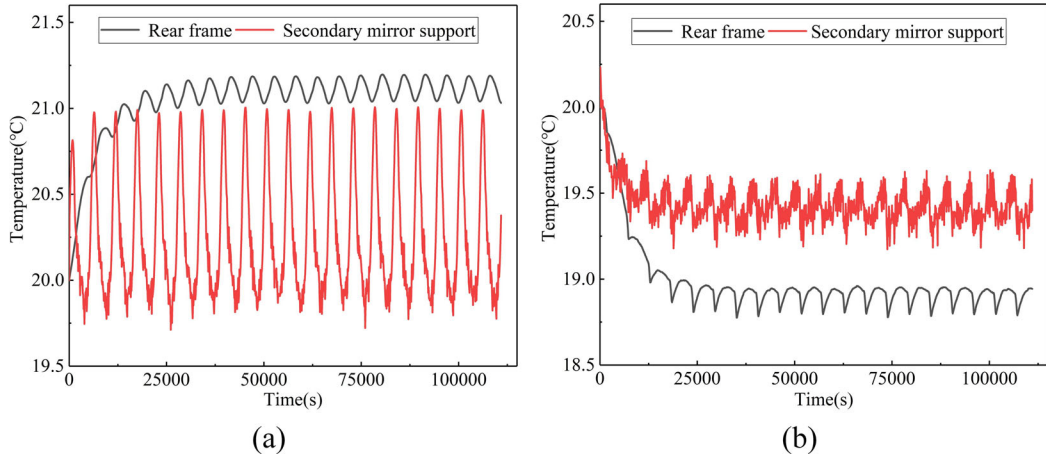
where $D_{i,j}$ is the heat transfer coefficient between node i and j ; m and n respectively represent the number of nodes that have radiative heat exchange and conduction heat exchange with node j .

5.1.2. Definition of thermal analysis cases

The temperature of the telescope is not only affected by the flight attitude and β angle, but also the result of the superposition of many other factors. For example, the thermal property of anti-atomic oxygen cloth on MLI surface at the beginning of its life is $\alpha/\varepsilon = 0.22/0.84$, the thermal property at the end of life is $\alpha/\varepsilon = 0.3/0.84$. The thermal property of S781 white paint sprayed on radiant cold plate at the beginning of its life is $\alpha/\varepsilon = 0.17/0.86$, the thermal property at the end of life is $\alpha/\varepsilon = 0.35/0.86$. The solar constant S has a maximum value of $1412\text{W}/\text{m}^2$ at the winter solstice and a minimum value of $1322\text{W}/\text{m}^2$ at the summer solstice. And load cabin temperature and bottom cold plate temperature. The thermal analysis considers two extreme thermal transient cases and superimposes all the worst factors, as shown in Table 2.

Table 2. Definition of thermal analysis cases.

Thermal analysis cases	Hot case	Cold case
Flight attitude ($^{\circ}$)	Pitch angle 0, roll angle 0	Roll angle $+10$, Pitch angle 0
β ($^{\circ}$)	0	$+66$
MLI α/ε	0.3/0.84	0.22/0.84
S781 α/ε	0.35/0.86	0.17/0.86
S (W/m^2)	1412	1322
Load cabin ($^{\circ}\text{C}$)	40	-20
Bottom cold plate ($^{\circ}\text{C}$)	26	0

**Figure 7.** Temperature change curve of supporting structures: (a) hot case, (b) cold case.

5.1.3. Calculation results of thermal analysis

According to the definition of hot case and cold case, the transient thermal analysis and calculation of two cases are carried out. The space ambient temperature is set to 4 K, the initial temperature of the telescope is assumed to be 20°C , and the calculation time is 20 orbital cycles.

Figure 7(a) and 7(b) shows the temperature change curve of the supporting structure under hot and cold case respectively. Due to the good heat insulation effect of the telescope support and a series of thermal control measures adopted, the temperature of the rear frame and the secondary mirror support is maintained at $20 \pm 2^{\circ}\text{C}$. In fact, there is a small temperature gradient in the secondary mirror support due to the different pasting positions, different power consumption and working time of the heating sheet on the secondary mirror support.

Figure 8(a) shows the temperature nephogram of the optical element at a certain time under hot case, and Figure 8(b) draws the temperature change curve of the optical element in 20 orbital cycles. It can be seen from Figure 8 that the temperature of the primary mirror is within $20 \pm 0.5^{\circ}\text{C}$, the temperature of the secondary mirror is within $20 \pm 0.2^{\circ}\text{C}$, and the temperature of the other mirror groups does not exceed 21.3°C .

Figure 9(a) shows the temperature nephogram of the optical element at a certain moment under cold case, and Figure 9(b) plots the temperature change curve of the optical element during 20 orbital cycles. It can be seen from Figure 9 that the temperature of the primary mirror is stable at $18.6 \pm 1.5^{\circ}\text{C}$, the temperature of the secondary mirror is within $19.6 \pm 0.1^{\circ}\text{C}$, the temperature of the third mirror is within $19.0\text{--}19.1^{\circ}\text{C}$, and the temperature of the remaining mirror groups is not lower than 18.4°C .

The temperature change curve of the CCD under hot and cold case is shown in Figure 10. It can be seen from Figure 10 that due to the CCD generates a large amount of heat in a short time, the temperature fluctuates greatly. Under hot case, because the large external heat flow

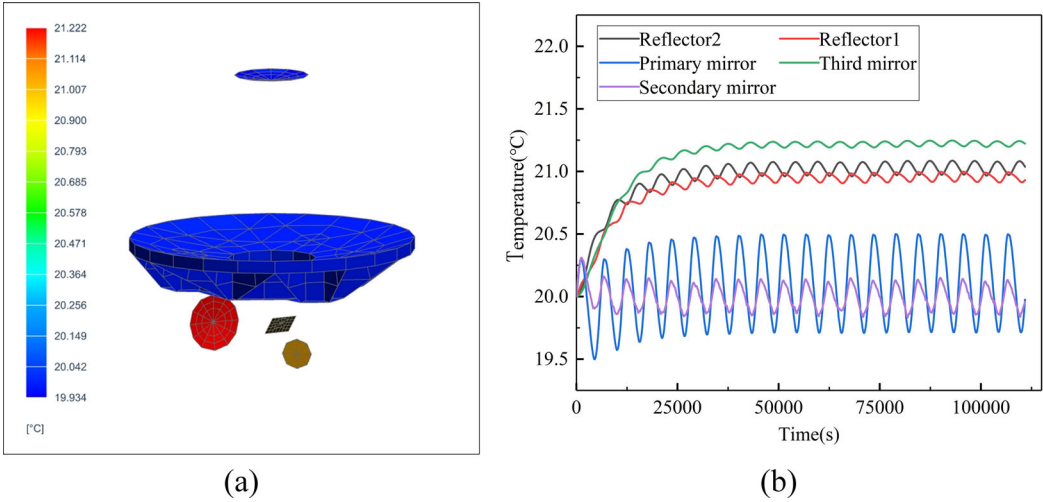


Figure 8. Optical elements under hot case: (a) temperature nephogram, (b) temperature change curve.

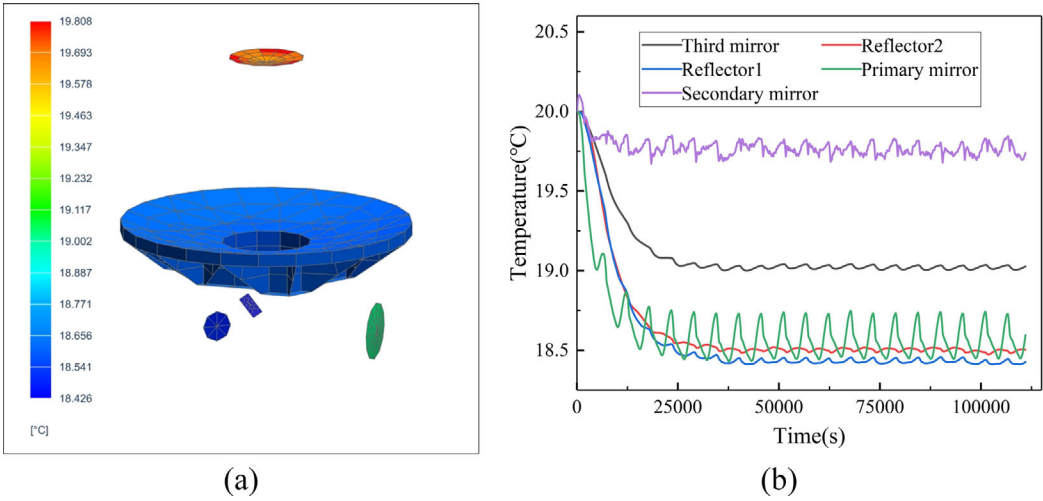


Figure 9. Optical elements under cold case: (a) temperature nephogram, (b) temperature change curve.

received by the heat dissipation surface, the temperature level of the CCD is relatively higher, but it satisfies the requirement of a working temperature of 0–30 °C.

Figure 11 shows the temperature change curve of the electric box under hot and cold case and it can be seen that the temperature of the electric box is higher under hot case, because the temperature of the bottom cold plate is as high as 28 °C, and the excess heat can not be dissipated in time. However, the overall temperature of the electric box meets the working requirements of –10–40 °C under the two cases.

The thermal analysis results show that the thermal control system can ensure that the key components of the telescope system meet its operating temperature requirements.

5.2. Structural analysis

In order to further analyze the deformation of the telescope under the predicted temperature field, the temperature results at a certain time under hot and cold case are taken as thermal

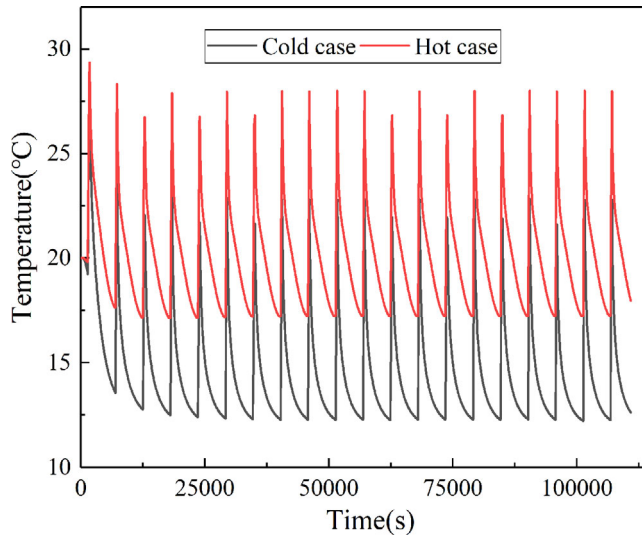


Figure 10. Temperature change curve of CCD.

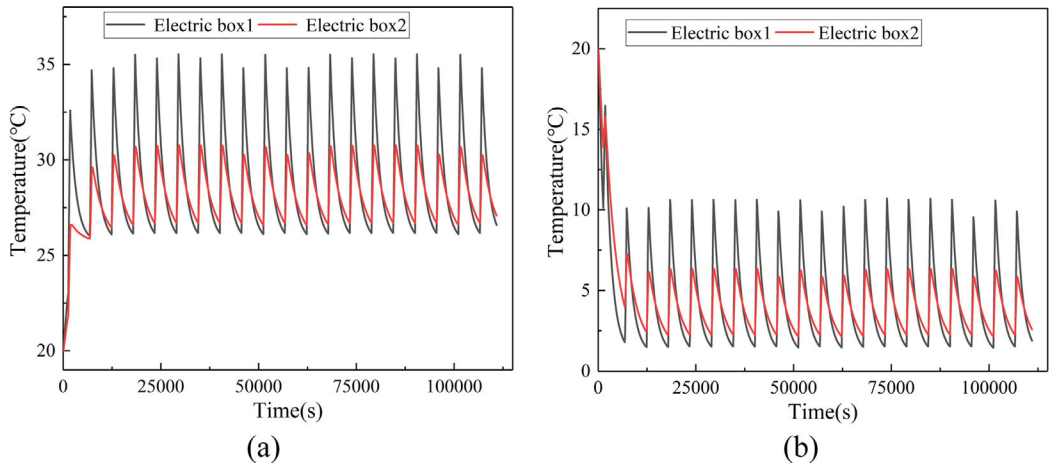


Figure 11. Temperature change curve of electric boxes: (a) hot case, (b) cold case.

boundary conditions and mapped into the structural model. Because the primary mirror is the most critical optical element of the telescope optical system, the temperature field under hot case takes the time when the primary mirror temperature is the highest, $t_1 = 79,000$ s, and the temperature field under cold case takes the time when the primary mirror temperature is the lowest, $t_2 = 43,200$ s.

The finite element model of the optical elements and main supporting structure of the telescope is established by UG/NX. The temperature fields at the selected hot and cold case are respectively mapped to the structural model. It is assumed that the thermal expansion coefficient of the material is constant and the reference temperature of the material is 20°C . The thermal deformation of the telescope optical system can be simply calculated by formula (6).

$$\Delta l = \Delta T \cdot L \cdot \alpha_{CTE} \quad (6)$$

where Δl is the deformation, ΔT is the temperature difference, L is the total length, α_{CTE} is the coefficient of thermal expansion of the material.

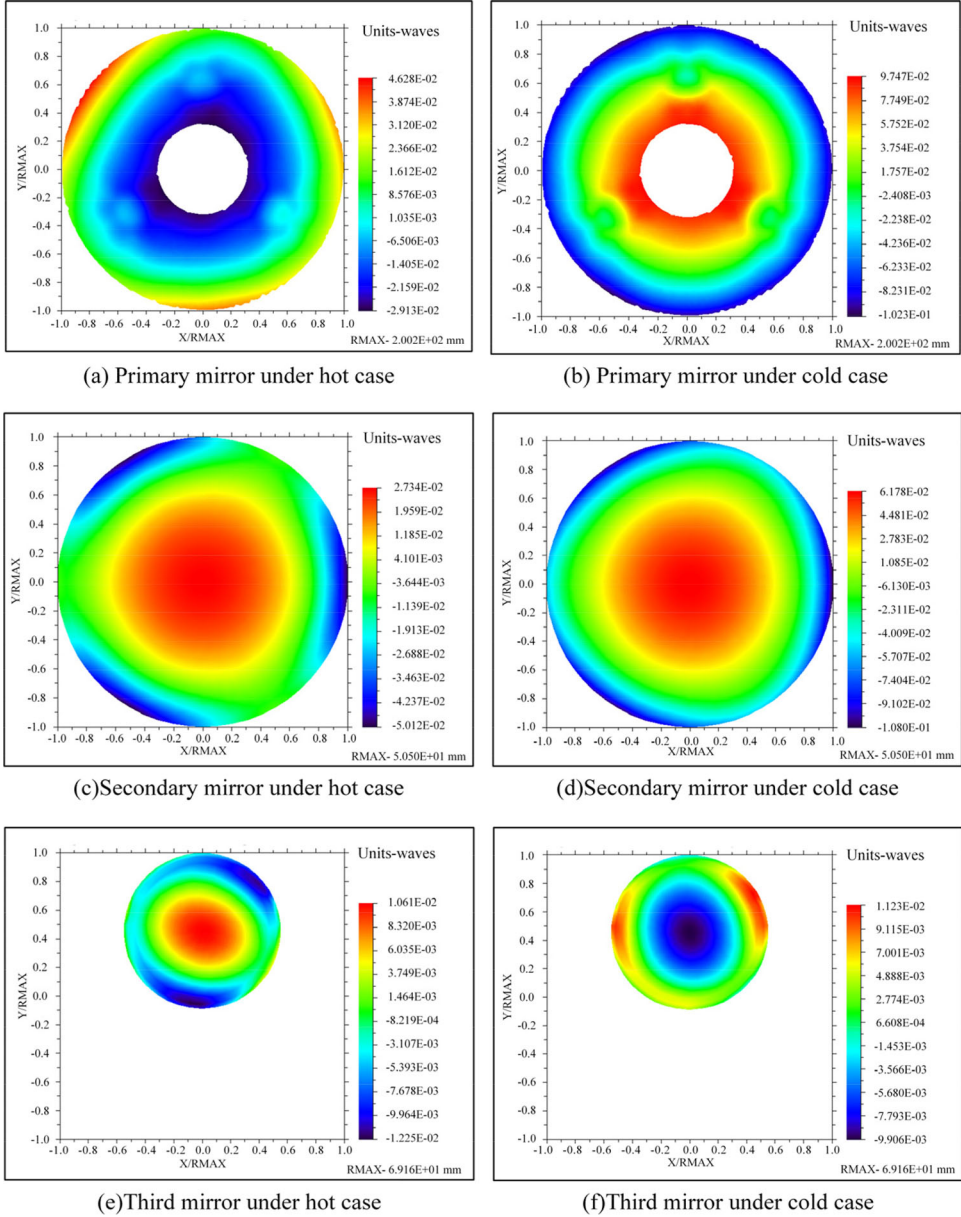


Figure 12. Mirror deformation after removing rigid body displacement.

Table 3. Rigid body displacement of optical elements.

Case	Optical elements	$dx(mm)$	$dy(mm)$	$dz(mm)$	$Rx(rad)$	$Ry(rad)$	$Rz(rad)$
Hot case	Primary mirror	$-6.789e-5$	$-1.404e-4$	$-4.751e-3$	$-1.269e-6$	$-7.023e-8$	$6.633e-7$
	Secondary mirror	$4.449e-4$	$-1.936e-4$	$-4.806e-3$	$-2.725e-7$	$-9.559e-7$	$3.919e-7$
	Reflector1	$2.502e-4$	$3.492e-3$	$-2.530e-3$	$-3.087e-6$	$-9.886e-7$	$1.913e-6$
	Third mirror	$6.294e-5$	$4.036e-3$	$-7.943e-4$	$-2.190e-6$	$1.744e-6$	$4.529e-7$
	Reflector2	$4.764e-4$	$4.280e-3$	$3.898e-4$	$-2.814e-6$	$-2.495e-6$	$2.820e-6$
Cold case	Primary mirror	$-5.751e-4$	$-1.443e-4$	$1.130e-2$	$-2.131e-6$	$5.066e-6$	$-9.203e-7$
	Secondary mirror	$1.707e-5$	$-4.800e-4$	$1.278e-2$	$3.027e-7$	$3.211e-6$	$-1.327e-6$
	Reflector1	$1.096e-4$	$-7.942e-3$	$6.175e-3$	$-3.807e-6$	$-1.748e-6$	$1.869e-6$
	Third mirror	$-2.466e-4$	$-1.059e-2$	$-4.615e-5$	$-1.571e-6$	$1.308e-6$	$-2.684e-7$
	Reflector2	$-6.960e-4$	$-9.434e-3$	$-7.094e-4$	$-1.152e-5$	$-3.993e-6$	$2.580e-6$

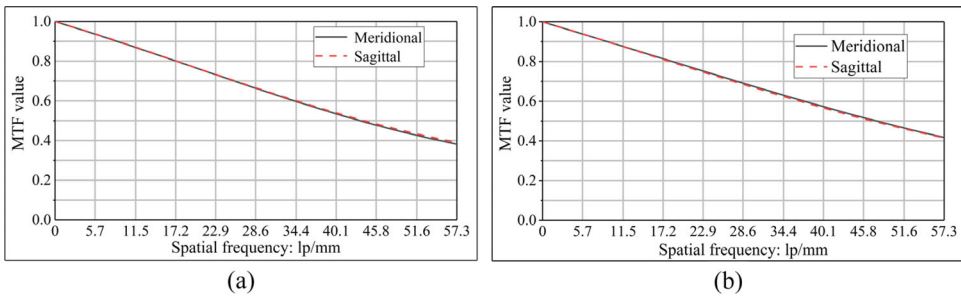


Figure 13. Average MTF of the optical system: (a) hot case, (b) cold case.

The results of structural analysis are usually used as the intermediate term of thermal/structural/optical analysis, which can not directly explain the performance of optical system [14]. The deformation and displacement of the optical system calculated by UG/NX are imported into SIGFIT. Then, the surface of the deformed optical element is fitted, and the rigid body displacement of the optical element is removed, which is simplified to the Zernike coefficient terms. The surface deformation of the optical element under hot and cold case after removing the rigid body displacement is shown in Figure 12, and the rigid body displacement of each optical element is given in Table 3.

5.3. Optical analysis

The Zernike coefficient terms and the rigid body displacement of the optical element (these are errors caused by heat) calculated above are imported into ZEMAX and combined into the original optical model to analyze the optical performance of the optical system under hot and cold case. It is assumed that the wavelength of the main light of the optical system is 900 nm and the cutoff frequency is 57.3 lp/mm. The average MTF curves of 12 fields of view are obtained through analysis and calculation, as shown in Figure 13.

It can be seen from Figure 13 that under hot case, the average MTF value of sagittal plane at cutoff frequency is 0.39 and that of meridional plane is 0.38. Under cold case, the average MTF values of sagittal plane and meridional plane at the cutoff frequency are 0.42.

The optical analysis results show that the average MTF at the cutoff frequency of all fields of view of the optical system under two cases meets the design requirements of more than 0.3.

6. Conclusion

According to the mission environment and working requirements of a space telescope, a set of thermal control system based on the combination of active and passive is designed, which makes full use of passive thermal control measures such as heat conduction, heat insulation and heat dissipation, combined with thermal compensation measures such as pasting heating sheets. By comprehensively considering the space thermal environment of the telescope and all the worst factors, two extreme working conditions are analyzed, including hot case and cold case. The thermal analysis results show that under the action of the thermal control system designed in this paper, the temperature of CCD under hot case is 16–28 °C, and the temperature under cold case is 12.5–22.5 °C, which meets its thermal control index. The electronic components meet the thermal control index of –10–40 °C under hot and cold case. In addition, the temperature of all optical elements is maintained at 20 ± 2 °C. Structural analysis and optical analysis are used to predict the optical performance of the telescope optical system under the temperature field predicted by thermal analysis, so as to further verify the rationality of thermal design. The results show that under hot case, the average MTF value of sagittal plane and meridional plane at cutoff

frequency is 0.39 and 0.38 respectively. Under cold case, the average MTF values of sagittal plane and meridional plane at the cutoff frequency are 0.42. It meets the design requirements that the average MTF at the cutoff frequency is greater than 0.3, which ensures the optical performance of the telescope, and verifies the rationality of the thermal design.

Disclosure statement

No conflict of interest exists in the submission of this manuscript, and manuscript is approved by all authors for publication.

Funding

This work was supported by National Key R&D Program of China, and 2018YFB0504800 (2018YFB0504801) is a project number.

ORCID

Zhipeng Yuan  <http://orcid.org/0000-0002-6435-3468>

Liheng Chen  <http://orcid.org/0000-0002-9904-3080>

References

- [1] C. J. Zhang, X. H. Xi, Y. X. Wang, J. Q. Zhu, and Y. J. Guan, "Structural optimization design of large aperture mirror for space remote sensing camera," *Infrared Laser Eng.*, vol. 49, p. 0214002, 2020. DOI: [10.3788/IRLA202049.0214002](https://doi.org/10.3788/IRLA202049.0214002).
- [2] W. Y. Liu, et al., "Developing a thermal control strategy with the method of integrated analysis and experimental verification," *Optik*, vol. 126, no. 20, pp. 2378–2382, 2015. DOI: [10.1016/j.ijleo.2015.05.138](https://doi.org/10.1016/j.ijleo.2015.05.138).
- [3] S. Redmond, S. Benton, A. M. Brown, P. Clark, et al., "Auto-tuned thermal control on stratospheric balloon experiments," *Ground-Based and Airborne Telescopes VII*, International Society for Optics and Photonics, 2018, p. 107005R. DOI: [10.1117/12.2312339](https://doi.org/10.1117/12.2312339).
- [4] H. R. Wang, et al., "A comparative study of the thermal performance of primary mirror at the four typical sites," *Optik*, vol. 174, pp. 727–738, 2018. DOI: [10.1016/j.ijleo.2018.05.008](https://doi.org/10.1016/j.ijleo.2018.05.008).
- [5] Y. Gao, B. Zhang, L. H. Chen, B. Q. Xu, and G. C. Gu, "Thermal design and analysis of the high resolution MWIR/LWIR aerial camera," *Optik*, vol. 179, pp. 37–46, 2019. DOI: [10.1016/j.ijleo.2018.09.187](https://doi.org/10.1016/j.ijleo.2018.09.187).
- [6] S. Q. Li, Y. Wang, H. Zhang, F. Yu, "Thermal analysis and validation of GF-4 remote sensing camera," *J. Therm. Sci.*, vol. 29, no. 4, pp. 992–1000, 2020. DOI: [10.1007/s11630-020-1230-5](https://doi.org/10.1007/s11630-020-1230-5).
- [7] M. Mueller, et al., "Precision thermal control of the GMT-consortium large earth finder (G-CLEF)," *Ground-Based and Airborne Instrumentation for Astronomy VII*, International Society for Optics and Photonics, 2018, p. 10702A10702. DOI: [10.1117/12.2314038](https://doi.org/10.1117/12.2314038).
- [8] S. J. Li, L. H. Chen, W. T. Feng, and Y. H. Wu, "Calculation of external heat fluxes on space camera with two-dimensional changing attitudes in sun-synchronous orbit," *Infrared Laser Eng.*, vol. 47, p. 917008, 2018.
- [9] S. J. Li, L. H. Chen, and Y. H. Wu, "Thermal design of detector for the solar X-ray and extreme ultraviolet imager," *J. Thermophys. Heat Transf.*, vol. 33, no. 2, pp. 285–291, 2019. DOI: [10.2514/1.T5423](https://doi.org/10.2514/1.T5423).
- [10] S. J. Li, L. H. Chen, and Y. T. Yang, "Thermal design and test verification of the solar X-Ray and extreme ultraviolet imager," *Optik*, vol. 203, p. 164017, 2020. DOI: [10.1016/j.ijleo.2019.164017](https://doi.org/10.1016/j.ijleo.2019.164017).
- [11] B. Cullimore, T. Panczak, J. Baumann, et al., "Automated multidisciplinary optimization of a space-based telescope," *SAE Trans.*, vol. 111, pp. 288–296, 2002. DOI: [10.4271/2002-01-2445](https://doi.org/10.4271/2002-01-2445).
- [12] C. L. Li, Y. L. Ding, C. Lin, Y. F. Wei, Y. Q. Zheng, and L. Zhang, "Optomechanical design and simulation of a cryogenic infrared spectrometer," *Appl. Opt.*, vol. 59, no. 15, pp. 4642–4649, 2020. DOI: [10.1364/AO.392621](https://doi.org/10.1364/AO.392621).
- [13] Y. H. Wu, L. H. Chen, H. Li, S. J. Li, and Y. T. Yang, "Computation of external heat fluxes on space camera with attitude change in geostationary orbit," *Infrared Laser Eng.*, vol. 48, no. 9, p. 604001, 2019.
- [14] M. Borden, D. Lewis, H. Ochoa, et al., "Thermal, structural, and optical analysis of a balloon-based imaging system," *PASP*, vol. 129, no. 973, p. 035001, 2017. DOI: [10.1088/1538-3873/129/973/035001](https://doi.org/10.1088/1538-3873/129/973/035001).